Title: Widespread ripples synchronize human cortical activity during sleep, waking, and memory recall

Authors: Charles W. Dickey[1,2,*], Ilya A. Verzhbinsky[2], Xi Jiang[1], Burke Q. Rosen[1], Sophie Kajfez[3], Brittany Stedelin[4], Jerry J. Shih[5], Sharona Ben-Haim[6], Ahmed M. Raslan[4], Emad N. Eskandar[7], Jorge Gonzalez-Martinez[8], Sydney S. Cash[9], Eric Halgren[3,5,*]

Affiliations:
[1]Neurosciences Graduate Program, University of California San Diego, La Jolla, CA 92093, USA
[2]Medical Scientist Training Program, University of California San Diego, La Jolla, CA 92093, USA
[3]Department of Radiology, University of California San Diego, La Jolla, CA 92093, USA
[4]Department of Neurological Surgery, Oregon Health & Science University, Portland, OR 97239, USA
[5]Department of Neurosciences, University of California San Diego, La Jolla, CA 92093, USA
[6]Department of Neurological Surgery, University of California San Diego, La Jolla, CA 92093, USA
[7]Department of Neurological Surgery, Montefiore Medical Center, Albert Einstein College of Medicine, Bronx, NY 10461, USA
[8]Epilepsy Center, Cleveland Clinic, Cleveland, OH 44106
[9]Department of Neurology, Massachusetts General Hospital, Harvard Medical School, Boston, MA 02114, USA
*Corresponding authors: Eric Halgren (ehalgren@health.ucsd.edu), Charles W. Dickey (cdickey@health.ucsd.edu)

Acknowledgements: We thank Adam Niese, Christine Smith, Christopher Gonzalez, Daniel Cleary, Eran Mukamel, Erik Kaestner, Jacob Garrett, Maxim Bazhenov, Terrence Sejnowski, and Zarek Siegel for their support. This work was supported by NIMH (1RF1MH117155-01, T32 MH020002) and ONR-MURI (N00014-16-1-2829).

Author contributions: C.D. and E.H. designed the study. C.D., B.S., J.S., S.B., A.R., E.E., J.G., and S.C. collected the data. C.D., I.V., and X.J. analyzed the data. B.R. and S.K. provided support for the analyses. C.D. and E.H. wrote the manuscript. E.H. supervised the work.

Competing interests: The authors declare no competing interests.

Abstract

Declarative memory encoding, consolidation, and retrieval require the integration of elements encoded in widespread cortical locations. The mechanism whereby such 'binding' of different components of mental events into unified representations occurs is unknown. The 'binding-by-synchrony' theory proposes that distributed encoding areas are bound by synchronous oscillations enabling enhanced communication. However, evidence for such oscillations is sparse. Brief high-frequency oscillations ('ripples') occur in the hippocampus and cortex, and help organize memory recall and consolidation. Here, using intracranial recordings in humans, we report that these ~70ms duration 80Hz ripples often couple (within ±500ms), co-occur (≥25ms overlap), and crucially, phase-lock (have consistent phase-lags) between widely distributed focal cortical locations during both sleep and waking, even between hemispheres. Cortical ripple co-occurrence is facilitated through activation across multiple sites, and phase-locking increases with more cortical sites co-rippling. Ripples in all cortical areas co-occur with hippocampal ripples but do not phase-lock with them, further suggesting that cortico-cortical synchrony is mediated by cortico-cortical connections. Ripple phase-lags vary across sleep nights, consistent with participation in different networks. During waking, we show that hippocampo-cortical and cortico-cortical co-ripples increase preceding successful delayed memory recall, when binding between the cue and response is essential. Ripples increase and phase-modulate unit-firing, and co-ripples increase high-frequency correlations between areas, suggesting synchronized unit-spiking facilitating information exchange. Co-occurrence, phase-synchrony, and high-frequency correlation are maintained with little decrement over very long distances (25cm). Hippocampo-cortico-cortical co-ripples appear to possess the essential properties necessary to support binding-by-synchrony during memory retrieval, and perhaps generally.

Introduction

Ripples are brief high-frequency oscillations that have been well-studied in rodent hippocampus during non-rapid eye movement sleep (NREM), when they mark the replay of events from the previous waking period, and are critical for memory consolidation in the cortex (1-4). Recently, ripples were found in rat association cortex but not primary sensory or motor cortices during sleep, with increased coupling to hippocampal ripples in sleep following learning (5). An earlier study reported ripples in waking and sleeping cat cortex, especially NREM (6). In humans, cortical ripples have recently been identified during waking, and were more frequently found in lateral temporal than rolandic cortex. Hippocampal sharpwave-ripple occurrence and ripple coupling between parahippocampal gyrus and temporal association cortex are increased preceding memory recall in humans (7, 8), possibly facilitated through the replay of cortical neuron firing sequences established during encoding (9). In rats, ripples co-occur between hippocampus and ~1mm^2 of parietal cortex in sleep following learning (5), in mice, ripples propagate from the hippocampus to retrosplenial cortex (10), and in cats, ripple co-occurrence is reportedly limited to short distances (6).

We recently reported, using human intracranial recordings, that ~70ms long ~80Hz ripples are ubiquitous in all regions of the cortex during NREM as well as waking (11). During waking, cortical ripples occur on local high frequency activity peaks. During sleep, cortical ripples occur, often during spindles, and typically on the down-to-upstate transition, with unit-firing patterns consistent with generation by pyramidal-interneuron feedback. We found that cortical ripples mark the recurrence of spatiotemporal activity patterns from preceding waking, and they group

co-firing within the window of spike-timing-dependent plasticity. These findings are consistent with cortical ripples contributing to memory consolidation during NREM in humans.

While there is thus an emerging appreciation that hippocampal and cortical ripples have an important role in memory in humans and rodents, nothing is known of the network properties of cortical ripples. Specifically, it is not known if ripples co-occur or phase-synchronize between cortical sites, and if so, whether this is affected by distance or correlated with the reconstruction of declarative memories. These would be critical properties for cortical ripples to participate in the binding of different elements of memories that are represented in disparate cortical areas, the essence of hippocampus-dependent memory (12).

The binding of disparate elements of a memory is a specific case of a more general problem of how the various contents of a mental event are united into a single experience. Most often addressed is how different visual qualities of an object (e.g., color, shape, location, texture) are associated with each other (13), but the 'binding problem' generalizes to how the contents of awareness are unified in a single stream of consciousness (14). Modern accounts often rely on hierarchical and multimodal convergence. However, cortical processing is distributed, and it would be difficult to represent the combinatorial possibilities contained in all potential experiences with convergence, leading to the suggestion that temporal synchrony binds cortical areas (15). This hypothesis was first supported by phase-locked unit-firing and local field potentials (LFP) at 40-60Hz evoked by simple visual stimuli in the anesthetized cat primary visual cortex at distances <7mm (16). Although some further studies found similar results in other cortical areas, behaviors and species, as would be expected under the binding-by-synchrony hypothesis (17, 18), others have been less successful (19). Synchronous high gamma oscillations have also been criticized as providing no mechanism for neuronal interaction beyond generic activation (19, 20).

Here, using human intracranial stereoelectroencephalography (SEEG) recordings, we find that ripples co-occur, and remarkably, phase-synchronize across all lobes and between both hemispheres, with little decrement, even at long distances. Furthermore, ripple co-occurrence is enhanced between cortical sites as well as between the cortex and hippocampus preceding successful delayed recall. Co-rippling was progressively above that expected as it involved a larger proportion of sites, and this led to progressively stronger phase-locking. Single-unit firing increased during, and phase-locked to, cortical ripples, providing a basic requirement for ripples to enhance communication via gain-modulation and coincidence detection. Enhanced communication was supported by our finding of increased high-frequency correlation between even distant co-rippling regions. These characteristics suggest that distributed, phase-locked cortical ripples possess the properties that may allow them to help integrate different components of a memory. More generally, ripples may help to 'bind' different aspects of a mental event encoded in widespread cortical areas into a coherent representation.

Results

Ripple detection during NREM and waking

Ripples were detected using intracranial cortical and hippocampal recordings in 17 patients (STable 1) undergoing monitoring to localize seizure foci during NREM and waking. Bipolar contact derivations were used to measure local field potentials (LFP). Ripples were detected only on channels in non-lesional, non-epileptogenic areas. Ripples were required to have 3 or more cycles of increased 70-100Hz amplitude that did not contain epileptiform activity or artifacts. Ripples were also required not to occur at the time of putative interictal spikes detected

on any other channel to exclude events that could be spuriously coupled due to epileptiform activity.

Cortical ripples were detected in all lobes of both hemispheres during NREM and waking (Fig.1A-B). Cortical and hippocampal ripples were consistently ~70-85ms long ~80Hz oscillations (Fig.1A-B). Specifically, cortical ripples during NREM had an average and standard deviation density of 8.36±2.69min^{-1}, amplitude of 1.70±0.75μV, duration of 76.47±10.14ms, and frequency of 81.18±0.78Hz, and during waking had a density of 5.79±3.41min^{-1}, amplitude of 2.44±1.31μV, duration of 66.59±7.17ms, and frequency of 81.28±0.55Hz, with a strong association of high-frequency (>200Hz) amplitude during waking ripples (Fig.1C-D; *N*=273 channels). Hippocampal ripples during NREM had an average and standard deviation density of 6.95±4.80min^{-1}, amplitude of 5.76±2.58μV, duration of 87.46±9.05ms, and frequency of 78.50±1.34Hz, and during waking had a density of 7.40±5.47min^{-1}, amplitude of 6.00±3.16μV, duration of 69.74±7.91ms, and frequency of 80.29±0.85Hz (*N*=28 channels). A standard deviation of <1Hz in ripple frequency in all circumstances suggests the possibility that local channel and network properties underlie a consistent resonant frequency.

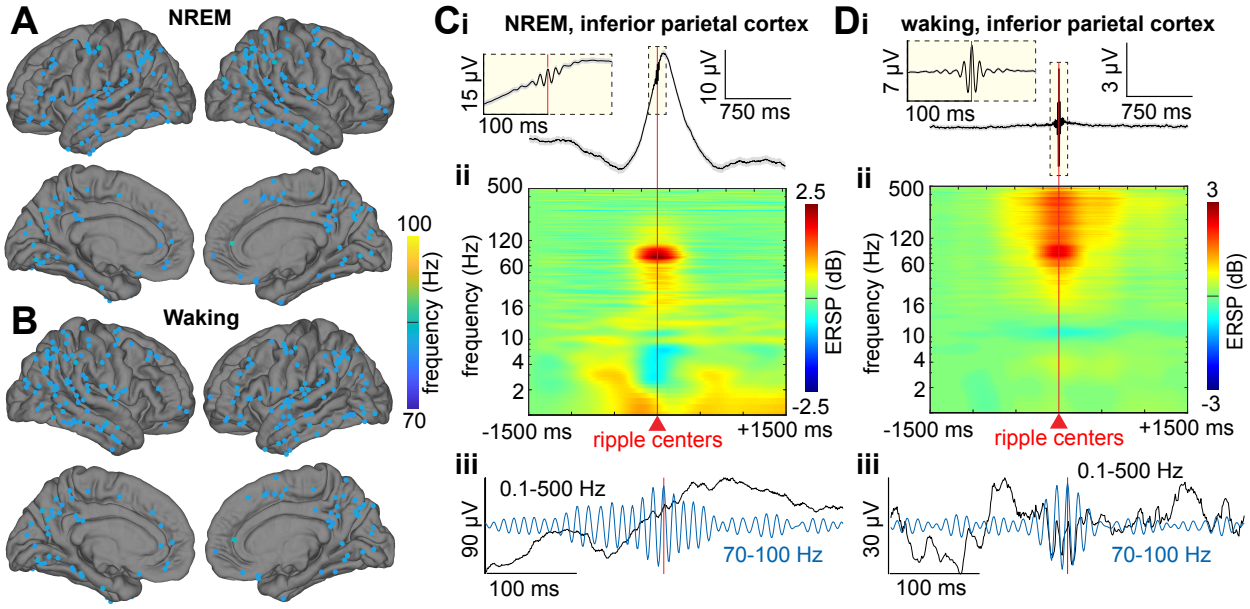

Fig. 1. Cortical ripple generation during NREM and waking. (**A**) Cortical ripple oscillation frequencies across the cortex during NREM. Each marker depicts the average ripple frequency in a given channel (*N*=273 channels from SEEG patients S1-17). Color range spans the ripple band used for detection (70-100Hz). Note the highly consistent frequencies across lobes, between hemispheres, and between NREM and waking. (**B**) Same as (A) except for waking. (**C**) Average broadband LFP (**i**) and time-frequency (**ii**) across cortical ripples, and example broadband ripple (**iii**) unfiltered single sweeps (black), and 70-100Hz bandpass (blue) during NREM. Recording is from a channel in inferior parietal cortex. (**D**) Same as (A) except inferior parietal cortex ripples during waking. Error shows SEM. SEEG=stereoelectroencephalgography, bipolar recordings.

Cortical ripples couple and co-occur across widespread regions

We hypothesized that ripples couple (defined here as occurrence within ±500ms) and even more importantly co-occur (≥25ms overlap) between cortical sites, which would be crucial for

widespread information integration. We discovered that cortical ripples frequently and strongly couple with each other during both NREM (N=4487/4550 significant channel pairs, randomization test, post-FDR p<0.05) and waking (N=4478/4550), between all cortical areas sampled (Fig.2A, Table 1), including between hemispheres. The proportion of cortico-cortical channel pairs that were significantly coupled during NREM (98.6%) was not significantly different than that proportion during waking (98.4%; p=0.44, χ^2=0.61, df=1).

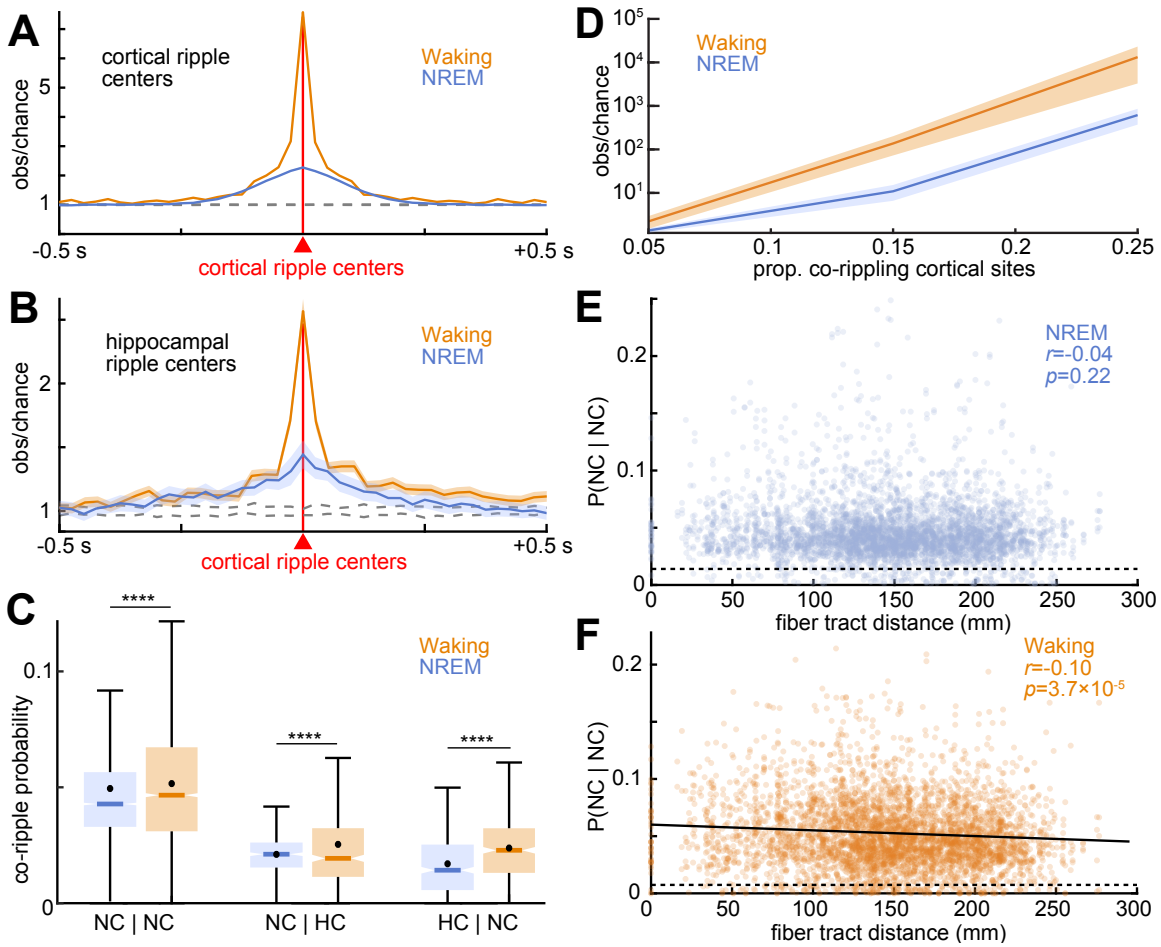

Fig. 2. Cortico-cortical and hippocampo-cortical ripples couple and co-occur during waking and NREM. (**A**) Cortico-cortical ripple time delays reveal strong coupling (occurring within 500ms of each other without necessarily overlapping) between nearly all sites during NREM (N=4487/4550 significant channel pairs) and waking (N=4478/4550; post-FDR p<0.05, randomization test). Dashed lines show 99% confidence interval of the null distribution (200 shuffles/channel pair). (**B**) Same as (A) except hippocampal ripple coupling with cortical ripples (NREM: N=133/461; waking: N=401/461). (**C**) Conditional co-occurrence probabilities of cortico-cortical and hippocampo-cortical ripples overlapping for at least 25ms (i.e., probability of a ripple in a particular channel given a ripple in another particular channel) are greater during waking than NREM (****post-FDR p<0.0001, two-sided paired t-test). (**D**) Observed over chance cortical ripple co-occurrence (logarithmic scale) increases with the number of sites co-rippling. (**E**) Cortical ripple co-occurrence probabilities during NREM are stable with increasing intervening fiber tract distance (linear mixed-effects with subject as random effect). Dashed line indicates chance. (**F**) Same as (E) except for waking. Fit is linear least-squares regression. Error shows SEM.

Ripple | Ripple	Significant Modulation	Significant Sidedness	Cortical Ripple Leading
	NREM		
Cort-R | Cort-R	98.62% (4487/4550)	3.50% (157/4487)	N/A
Hipp-R | Cort-R	28.85% (133/461)	31.58% (42/133)	33.33% (14/42)*
Cort-R | Hipp-R	29.28% (135/461)	31.11% (42/135)	33.33% (14/42)*
Hipp-SWR | Cort-R	19.74% (91/461)	45.05% (41/91)	24.39% (10/41)*
Cort-R | Hipp-SWR	20.61% (95/461)	44.21% (42/95)	21.43% (9/42)*
Hipp-SSR | Cort-R	12.15% (56/461)	17.85% (10/56)	50% (5/10)
Cort-R | Hipp-SSR	11.71% (54/461)	22.22% (11/54)	41.67% (5/12)
	Waking		
Cort-R | Cort-R	98.42% (4478/4550)	8.13% (364/4478)	N/A
Hipp-R | Cort-R	86.98% (401/461)	22.44% (90/401)	84.44% (76/90)*
Cort-R | Hipp-R	87.42% (403/461)	22.33% (90/403)	84.44% (76/90)*

Table 1. Cortical ripple coupling with cortical or hippocampal ripples: frequency and order. *Significant Modulation:* Proportion of channel pairs with a significant increase in the conditional probability of a ripple occurring in the first channel given that one occurred within ±500ms in the second (e.g., Hipp-R | Cort-R refers to hippocampal ripples occurring within ±500ms relative to cortical ripples at t=0; one-sided randomization test, 200 shuffles, 25ms non-overlapping bins, 3 consecutive bins with p<0.05 required for significance). During NREM, conditional probabilities are shown separately for those hippocampal ripples associated with sharpwaves (Hipp-SWR) and sleep spindles (Hipp-SSR) as well as all ripples (Hipp-R). *Significant Sidedness:* Those with significant modulations that had significant sidedness preference around t=0 (p<0.05, two-sided binomial test, expected=0.5, -500 to -1ms vs. 1 to 500ms). *Cortical Ripple Leading:* Those with significant sidedness around 0 that had cortical ripples leading (according to counts within -500 to -1ms vs. 1 to 500ms). During NREM, Hipp-R and Hipp-SWR led Cort-R, and during waking, Cort-R led Hipp-R (*=p<0.05, two-sided binomial test, expected value=0.5), resulting in a significant preference for cortical ripples to lead hippocampal ripples in waking vs. NREM (p<0.00001, χ^2=51.59, df=1).

Critically, we found that short latency coupling led to co-occurrence (≥25ms overlap) of these ~70ms long ripples, with slightly but significantly higher probabilities during waking than NREM (Fig.2C). The percent of cortico-cortical channel pairs with significant ripple co-occurrence was very high and nearly equal during NREM (N=2218/2275, 97.5%) vs. waking (N=2225/2275, 97.8%). Thus, nearly all cortico-cortical channel-pairs couple and co-occur above chance during both sleep and waking.

Hippocampal and cortical ripples couple and co-occur, especially during waking, but at lower rates than cortico-cortical

As previously found (8), ripples in many hippocampo-cortical channel-pairs were also significantly coupled (Fig.2B, Table 1) during both NREM (N=133/461) and waking (N=401/461), but at a significantly lower rate than cortico-cortical pairs in both states (NREM: p<0.00001, χ^2=2832.0, df=1; Waking: p<0.00001, χ^2=213.3, df=1). Unlike cortico-cortical pairs, the proportion of significant hippocampo-cortical pairs was higher during waking (87.0%) than NREM (28.9%, p<0.00001, χ^2=319.61, df=1). Of note, these findings of cortico-cortical and

hippocampo-cortical couplings were maintained when only cortical and hippocampal channels that were free of interictal spikes at any time were analyzed (STable 2).

Overlapping co-occurrence of human ripples between cortex and hippocampus do not appear to have been studied *per se*, but would also be expected to occur given their coupling. Indeed, we found significant co-occurrence of ripples in 81.1% (N=374/461) of hippocampo-cortical site-pairs during waking, and 34.7% (N=160/461) during NREM. Higher hippocampo-cortical co-occurrence during waking compared to NREM was significant ($p<0.00001$, $\chi^2=203.8$, df=1). In addition, these percentages for hippocampo-cortical co-occurrences (81.1% waking; 34.7% NREM) are significantly lower than for cortico-cortical site-pairs (97.5% waking; 97.8% NREM) (NREM: $p<0.00001$, $\chi^2=1328.8$, df=1; waking: $p<0.00001$, $\chi^2=1250.1$, df=1*).* Thus, ripples in hippocampal and cortical sites do couple and co-occur, but at a substantially lower rate than between cortical sites.

Hippocampal ripples lead cortical during NREM and *vice versa* during waking

The order of rippling in the hippocampus versus cortex is of interest, given the hypothesized transfer of information from hippocampus to cortex during sleep consolidation, and from cortex to hippocampus during waking memory encoding. During NREM, 31.58% (42/133) of the hippocampo-cortical pairs that were significantly coupled had a significant sidedness preference, where one channel's ripples led the other's (Table 1; post-FDR $p<0.05$, two-sided binomial test, expected value=0.05). Among these significant pairs, hippocampal ripples led cortical ripples in 66.7% (28/42). By contrast, during waking, 22.4% (90/401) of the pairs with significant coupling showed a sided preference, with cortical ripples leading hippocampal ripples in 84.4% (76/90). This overall preference for hippocampal ripples to lead cortical ripples during NREM, and *vice versa* during waking was highly significant ($p=4.3\times10^{-9}$, $\chi^2=34.5$, df=1).

In the above results, we considered all ripples that met our quality criteria. However, studies of ripples in rodent hippocampus commonly focus on ripples that occur on a slower sharpwave (2). In humans, anterior hippocampal ripples during NREM typically occur on sharpwaves (21), whereas posterior hippocampal ripples are often associated with spindles (22). Sharpwave-ripples have stronger associations with sleep waves in prefrontal cortex areas supporting contextual aspects of episodic memory, whereas spindle-ripples can phase-lock with spindles in parietal areas supporting detailed autobiographical recollection. Here, we found that hippocampal sharpwave-ripples significantly preceded cortical ripples by ~250ms (SFig.1A; p=0.002, two-sided binomial test, expected value=0.5), whereas spindle-ripples were concurrent (SFig.1B; p=1). These results reinforce a previous suggestion that ripples make sequential contributions to consolidation (22). Overall, as predicted by models of hippocampo-cortical interaction for memory, hippocampal ripples usually lead cortical during sleep, and cortical usually lead hippocampal during waking.

Cortical ripple co-occurrence is facilitated through activation across multiple sites

In each patient, we found that when two of the sampled cortical sites co-rippled, one or more additional sites could also be co-rippling (SFig.2). To test if two cortical sites co-rippling made it more likely for other sites also to co-ripple, we computed a χ^2 test of proportions for all possible groups of three cortical channels under the null hypothesis that the co-occurrence of channel A and B has no relation to the co-occurrence of A and C. We found that two sites co-rippling often made it more likely for another site to co-ripple, with an average of 14.1% of significant channel-triplets across patients during NREM and 38.8% during waking (patient specific results reported

in STable 3, χ^2 test of proportions, FDR-corrected *p*-values across channel-triplets within subjects).

In further support that co-rippling is facilitated through activation across multiple sites, we found that the level relative to chance for multiple locations to co-ripple increased with the number of locations co-rippling (>2) (Fig.2D). The increase was pronounced, such that the observed probability relative to baseline of 25% of all channels was ~10^4 during waking and ~5×10^3 during NREM. Thus, co-rippling appears to beget more co-rippling, suggesting the possibility of self-reinforcing spread.

Cortical ripples co-occur robustly across distance

Binding by ripples requires that they co-occur across widespread cortical areas. We compared conditional probabilities of cortico-cortical ripple co-occurrences (i.e., the probability of a ripple in one cortical site given a ripple in another cortical site, requiring ≥25ms overlap) against white-matter streamline distances between cortical sites. Streamline distances were computed using the 360 parcels of the HCP-MMP1.0 atlas (23), as determined by probabilistic diffusion MRI tractography (24), and are population averages from (25). We found that cortico-cortical co-rippling probability did not decrease with fiber tract distance during NREM (Fig.2E, r=-0.04, p=0.22, linear mixed-effects), but rather was maintained up to 25cm separation, across lobes and between hemispheres. During waking, co-rippling probabilities were also maintained across this distance range, albeit with a weak but significant negative linear relationship (Fig.2F, r=-0.10, $p=3.7\times10^{-5}$).

Ripples in all cortical areas co-occur with hippocampal ripples

It was previously reported that ripple coupling occurs between the parahippocampal gyrus and 16.4% of lateral temporal electrodes but only 3.3% of Rolandic (8). This seems to be consistent with the anatomical location of the hippocampus at the apex of the cortical hierararchy (26). However, we found that hippocampal ripples co-occurred with ripples in all cortical areas at approximately equal rates in both NREM and waking. Taking the myelination index as a measure of the location of different areas on the sensorimotor to association cortex hierarchy, in which association areas are less myelinated (27), we found a weak but significant effect during NREM but not waking. During NREM, hippocampo-cortical co-occurrence was positively correlated (r=0.15) with myelination (p=0.01), indicating that hippocampal ripples are slightly more likely to co-occur with ripples in primary cortical areas (SFig.3). Possibly, even if the hippocampus is more directly connected with high-level cortices, it indirectly co-ripples with all cortical areas via the dense cortico-cortical co-rippling networks described above.

Cortico-cortical and hippocampo-cortical ripple co-occurrences precede recall

If ripples in different cortical regions bind the elements of a memory, it would be expected that cortical ripples co-occur preceding cued recall, which requires that those elements be co-activated. To test this hypothesis, we analyzed paired-associates memory task data from 5 SEEG patients (Fig.3A, STables 1,4). Preceding delayed cued recall, there was a significant increase in cortical ripple occurrence ($p=1\times10^{-11}$) of 330% of chance, and an even greater increase in cortico-cortical ripple co-occurrence of 758% of chance (p=0.0004, linear mixed-effects; Fig.3B-E). Furthermore, cortical ripple occurrence (p=0.002) and cortico-cortical (p=0.002) and hippocampo-cortical (p=0.008) ripple co-occurrence modulations were greater preceding delayed vs. immediate recall, which shared the same stimuli and responses. Finally, cortico-cortical (p=0.04) and hippocampo-cortical (p=0.004) co-rippling was enhanced preceding

correct vs. incorrect delayed recall, which was not the case for cortical (p=0.08) or hippocampal (p=0.94) ripples generally. Delayed but not immediate recall of paired associates is severely impaired by hippocampal damage (12). These data demonstrate increased co-rippling between cortical sites and between the hippocampus and cortex during hippocampal-dependent retrieval of novel combinations of previously unrelated items. This finding supports the hypothesis that hippocampo-cortical and cortico-cortical co-rippling may contribute to the reconstruction of declarative memories in humans.

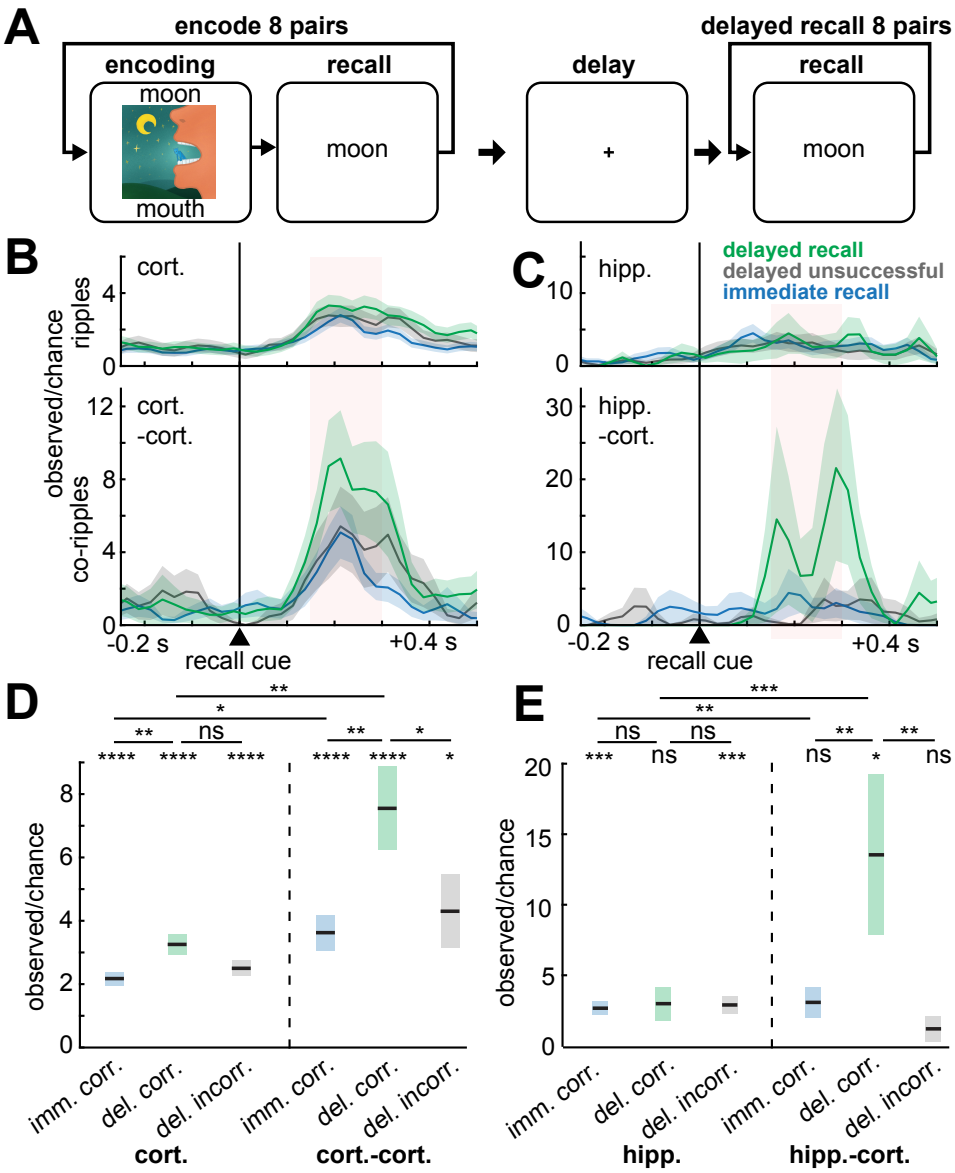

Fig. 3. Cortico-cortical and hippocampo-cortical ripple co-occurrences increase preceding recall. (**A**) Schematic of paired-associates memory task. Patients learned word pair associations and were subsequently cued with the first word to recall the second immediately following learning and then after a ~60s delay with distraction. (**B**) Cortical and cortico-cortical co-rippling increases following the stimulus cue triggering recall (delayed N=365 trials, immediate N=698 trials, patients S18-22). (**C**) Same as (B) except for hippocampal ripples and hippocampo-cortical co-ripples (delayed N=90 trials, immediate N=304 trials, patients S19,22).

(D-E) Quantification of (B-C) during the shaded 150-300ms interval following stimulus cue onset preceding correct recall in the immediate or delayed condition, or incorrect recall (no attempt or incorrect response) in the delayed condition. Note that cortico-cortical and hippocampo-cortical co-occurrences preceding correct delayed recall have the greatest increases. Errors show SEM. Post-FDR *p<0.05, **p<0.01, ***p<0.001, ****p<0.0001, linear mixed-effects models.

Cortical ripples phase-lock across widespread regions

Phase-locked oscillations in widespread locations have been hypothesized to underlie integration ('binding') of different components of events across the cortical surface. For each channel-pair, we calculated the phase-locking value (PLV), a measure of the consistency of 70-100Hz phases between sites, independent of amplitude (28), across all of their co-ripple events in either NREM or waking. We found significant PLV of co-occurring ripples between all sampled cortical regions, including between hemispheres, in both states (Fig.4A-C). Channel-pairs with significant PLV were more frequent during NREM than waking (Fig.4C, STable 5; post-FDR p<0.05, randomization test; non-significant results in SFig.4A-B). An example of consistent phase between two cortical locations across two co-ripples is shown in Fig.4A. For each channel-pair, PLV was measured at each latency relative to the center of their co-ripple (Fig.4B), and these time-courses were averaged across all significant channel-pairs (Fig.4C). The increased PLV lasted for the entire period when the sites were co-rippling, and arose abruptly from baseline. PLV time-course was remarkably similar across channel-pairs. During sleep 2106/2275 cortico-cortical channel pairs had more than 40 co-occurring ripples, required for a reliable PLV estimate. Of these, 26.3% (554/2106) had significant PLV modulations. During waking, 1939/2275 had more than 40 co-occurring ripples, and 13.9% (269/1939) of these had significant PLV modulations (STable 5). In summary, distant pairs of sites throughout the cortex were found to have consistent phases during co-ripples in both NREM and waking.

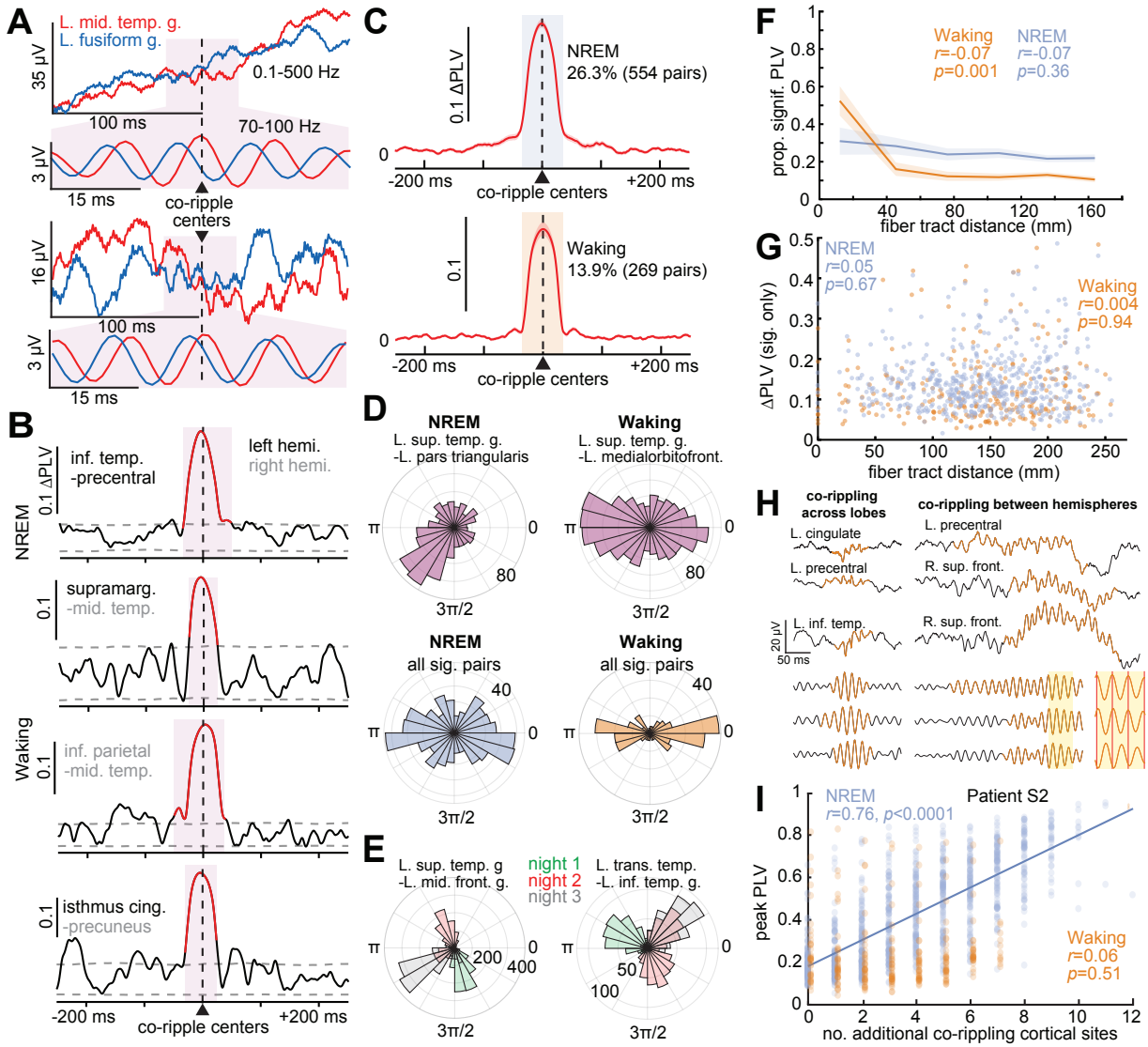

Fig. 4. Ripples phase-lock across wide separations in the cortex. (**A**) Two example pairs of co-occurring ripples in broadband LFP and 70-100Hz bandpass. A consistent phase-lag from the left middle temporal gyrus (red) to left fusiform gyrus (blue) is evident in the expanded bandpassed (70-100Hz) 50ms long traces centered on the co-ripple (pink background). Similar phase-lags were also present across other co-ripples between these sites, resulting in a significant PLV. (**B**) Example 70-100Hz PLV time-courses calculated between ripples co-occurring between ipsilateral and contralateral cortical sites (≥25ms overlap) in NREM and waking. Red shows significant modulation (post-FDR $p<0.05$, randomization test, 200 shuffles/channel pair). (**C**) Average ΔPLVs (relative to -500 to -250ms) for cortical channel pairs with significant PLV modulations. A greater percentage of pairs had significant co-ripple PLV modulations during NREM (26.3%) than waking (13.9%). (**D**) Polar histograms of waking and NREM 70-100Hz phase-lags across co-ripples for two example cortico-cortical pairs with significant PLV modulations (top) and across channel pair circular means (bottom). The magnitude of each pie-wedge corresponds to the number of co-ripples (top) or number of channel-pairs (bottom) with the indicated phase-lag. Cortico-cortical phase-lags had a significant preference for ~0 or ~π during waking compared to NREM based on the counts within 0±π/6 or π±π/6 vs. outside these ranges for NREM vs. waking ($p=5\times10^{-8}$, $\chi^2=29.75$,

df=1). (**E**) Example co-ripple phase-lag distributions for different sleep nights. The dominant phase-lag for co-ripples changes across nights (color-coded). (**F**) Proportion of channel pairs with significant PLVs has a weak, non-significant decrease over distance during NREM and a weak but significant decrease, notably at shorter distances, during waking. (**G**) ΔPLV does not decrement with intervening fiber tract distance for channel-pairs with significant PLVs (linear mixed-effects with subject as random effect). (**H**) Single sweep broadband LFP and normalized 70-100Hz bandpass show waking ripples (orange) co-occurring across lobes (left) and between hemispheres (right). Note the consistency of ~0 or ~π phases in the shaded inset. (**I**) Peak PLV correlates with the number of additional cortical sites co-rippling during NREM in a sample patient (N=10/17 patients significant, post-FDR $p<0.05$, significance of the correlation coefficient) more often than waking (N=3/17). Fit is linear least-squares regression. PLV=phase-locking value.

Phase-locked co-ripples have a broader range of phase-lags in NREM compared to waking and may vary across nights

Having demonstrated significant phase-locking between cortical co-rippling sites, we evaluated the distribution of the circular mean phase angles across site pairs. We found that during NREM the average phase angles for different cortical site-pairs that had significant co-ripple phase-locking had a fairly even distribution from 0 to 2π radians (Fig.4D left). However, during waking, co-ripple phase-lags across pairs tended to be ~0 or ~π (Fig.4D right). This difference was significant ($p=5\times10^{-8}$, $\chi^2=29.75$, df=1; using counts within 0±π/6 or π±π/6 vs. outside these ranges for NREM vs. waking). This observation suggests a greater tendency toward zero phase-lag during waking (we provide evidence below that the ~0 and ~π lags are functionally equivalent and may be due to a variability in fine-scale electrode contact placement relative to cortical layers). This may be related to the greater tendency of ripples to couple at near zero latency during waking (Fig.2A).

We also tested whether phase-lags during NREM varied across nights. For each patient with multiple sleep nights (N=16), we compared the co-ripple phase-lags between all possible pairs of sleep nights within channel pairs that had significant PLV modulations. We found that 42.0% (1256/2426) of such pairs were significantly different in their phase-lags between nights (Fig.4E; post-FDR $p<0.05$, Watson-Williams test; minimum 30 co-ripples per night per channel pair). These differences in co-ripple phase-lags between particular cortical sites suggest that they may participate in different networks across nights, as may happen, for example, when re-activating cortical representations associated with different memories. Similar phenomena have been noted in large-scale cortical models (29).

Ripples phase-lock robustly across long distances

Since declarative memories characteristically unite disparate elements that are encoded in widespread cortical locations in both hemispheres, any neurophysiological process supporting their encoding, consolidation, or retrieval must likewise function across those distances. Thus, given that cortico-cortical ripple co-occurrences do not decrement with distance (tested up to 200mm, Fig.2E-F), we hypothesized that cortico-cortical co-ripple phase-locking also does not decrement with distance. Indeed, we found that, like ripple co-occurrences, the proportion of channel-pairs with significant PLV modulations (Fig.4F; r=-0.07, p=0.36, linear mixed-effects) and the magnitude of these PLV modulations (Fig.4G; r=0.05, p=0.67) did not significantly decrement with intervening fiber tract distance during NREM. During waking, there was a significant decrement in the proportion of channel-pairs with significant PLV modulations with distance, more notably at shorter distances (Fig.4F; r=-0.07, p=0.001), but no decrement in the

magnitude of significant channel-pair PLV modulations with distance (Fig.4G; r=0.004, p=0.94). Thus, the physiological action supported by co-rippling may span the entire cortical surface.

Phase-locking increases with more cortical sites co-rippling

Ripples often phase-locked across multiple sites, including between hemispheres (Fig.4H), and as described above we found that two sites co-rippling made it more likely that a third site was co-rippling. These findings raise the question of whether activation of widespread co-rippling networks facilitates greater network synchronization. We found a strong positive linear correlation between the number of sites co-rippling and the cortico-cortical co-ripple phase-locking peak amplitude (Fig.4I). These results were again found when the ΔPLV (peak PLV minus baseline PLV) was used instead of the peak PLV (ΔPLV: N=7/17 patients significant during NREM, N=1/17 significant during waking, post-FDR p<0.05, significance of the correlation coefficient). Thus, the co-occurrence of ripples promotes further co-occurrence, which enhances phase-locking.

Hippocampo-cortical pairs rarely if ever phase-lock

Cortico-cortical phase-locking could be driven through a network of coupled cortical oscillators, a central driving mechanism, or a combination (Fig.6A). Since hippocampal ripples strongly co-occur with cortical ripples (Fig.2B), we investigated whether the hippocampus drives phase-locking of ripples in the cortex by testing if there is phase-locking between hippocampo-cortical co-ripples. For hippocampo-cortical pairs during sleep, 277/461 had more than 40 co-occurring ripples, and 1.4% (4/277) of these had significant PLV modulations. During waking, 333/461 of the hippocampo-cortical channel-pairs had more than 40 co-occurring ripples, and 0.3% (1/333) of these had a significant PLV modulation (SFig.4C-F; STable 5). Examination of electrode trajectories suggested that the hippocampal contacts with significant PLV with cortical sites were probably located in the subicular complex rather than the hippocampus proper, consistent with the finding in mice that ripple propagation from hippocampus to retrosplenial cortex is via the subiculum (10). Thus, it is unlikely that cortico-cortical ripple phase-locking is driven by common inputs from a hippocampal ripple, which supports the hypothesis that cortico-cortical co-ripple phase-locking is driven intracortically.

Cortical ripples are associated with increased and phase-modulated single unit firing

For ripples to have a role in the communication and integration of information between distant cortical sites requires that neuronal action-potentials coordinate with ripple occurrence and phase. We analyzed microarray recordings from human lateral temporal cortex granular/supragranular layers in 3 patients (STable 6) during NREM to test whether ripples modulate local single unit spiking. We detected spikes and sorted them into putative pyramidal (PY) and interneuron (IN) units based on waveform shapes and spike-timing characteristics, and verified that the units had large peak signal-to-noise ratios (PY: 9.12±3.39; IN: 5.23±2.88), had minimal interspike intervals that were <3ms (PY: 0.21±0.34%; IN: 0.33±0.58%; low percentages indicate minimal contamination by other units), and were well-isolated from one another based on the projection test (30) (PY: 95.38±86.00 SD; IN: 82.84±83.35 SD). We also detected ripples recorded by the array's microcontacts. We found that cortical ripples were associated with increased single unit-firing (Fig.5A-B). Putative pyramidal cells had a 315% increase and putative interneurons had a 345% increase in spiking during ripples compared to baseline (randomly selected epochs in between ripples that were matched in number and duration to the ripples). Furthermore, unit-firing was strongly phase-modulated by the ripples (Fig.5A), with 95% (68/73) of putative pyramidal cells and 86% (31/36) of putative interneurons

having significant 70-100Hz phase modulations during local ripples (Fig.5C; post-FDR $p<0.05$, binomial test between phases within 0±π/2 vs. π±π/2, expected value=0.5, minimum 30 spikes per unit across ripples). Thus, since unit spiking is coupled to the local ripple phase, and since ripple phases are synchronized at long distances, these data suggest that ripples coordinate unit spike-timing between wide separations in the cortex, which could enable phase selection, coincidence detection, re-entrant processing, and spike-timing-dependent plasticity (Fig.6B). These basic neurophysiological processes would influence the cooperative selection of cell-assemblies between cortical areas, the essence of binding.

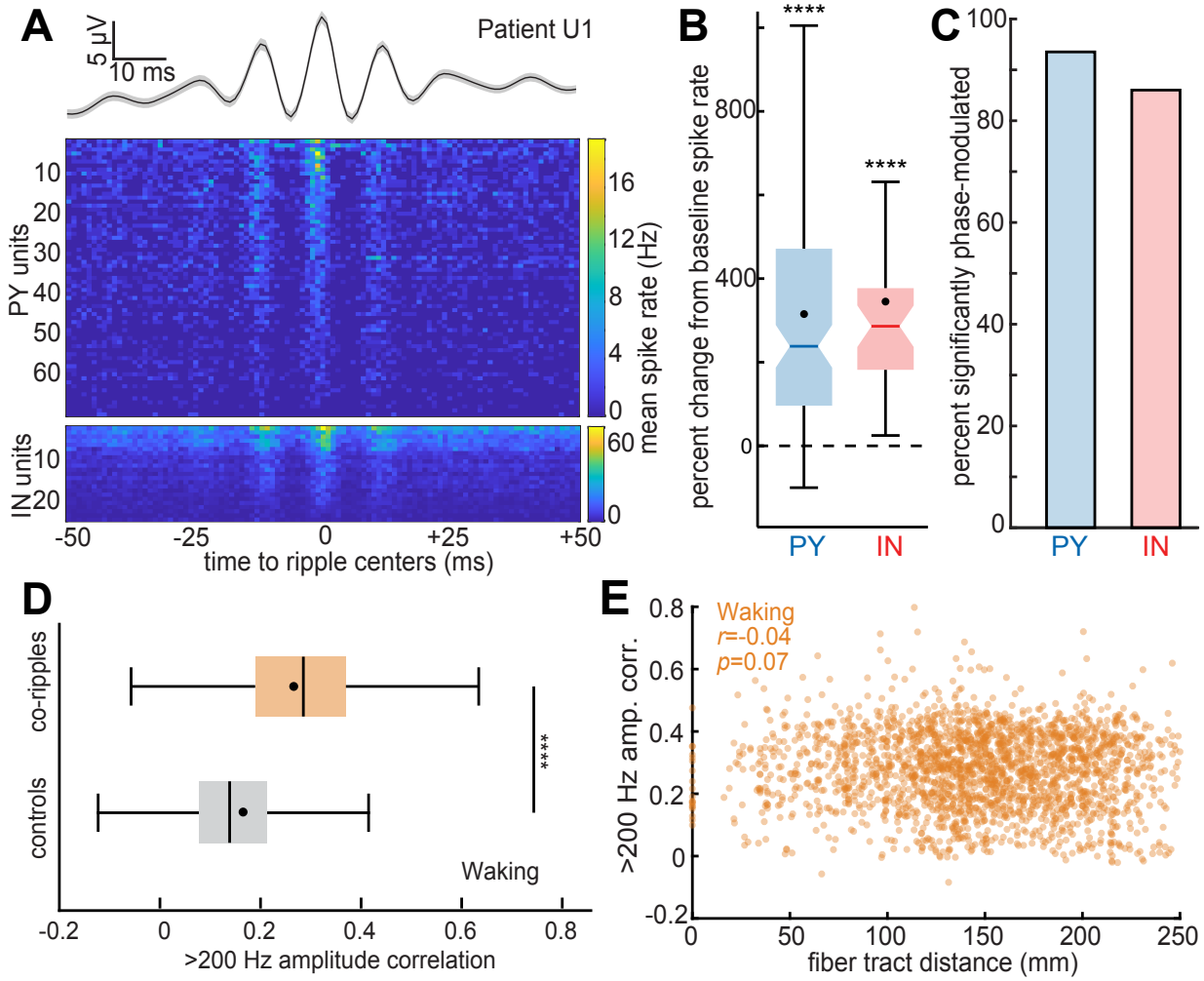

Fig. 5. Cortical ripples modulate local single unit spiking and synchronize high-frequency activity between distant regions. (**A**) Average cortical ripple broadband LFP and associated raster plot of pyramidal (PY) and interneuron (IN) mean spike rates across ripples during NREM. Note the phase-coupling of both PY and IN spiking to the ripple peaks. (**B**) Single unit spike rates increase during cortical ripples compared to baseline, which was comprised of randomly selected epochs in between ripples matched in number and duration (PY: N=133, mean=315%; IN: N=38, mean=345%; patients U1-3). (**C**) Single units are significantly phase-modulated by cortical ripples (PY: N=68/73 significant; IN: N=31/36 significant; binomial test between phases within 0±π/2 vs. π±π/2, expected value=0.5, minimum 30 spikes per unit across ripples). (**D**) Correlation of the >200Hz analytic amplitude, a proxy for unit spiking, increases during waking co-ripples compared to randomly selected preceding control periods

(within -10 to -2 s) matched in number and duration (*N*=2275 SEEG channel pairs). ****p<0.0001, two-sided paired *t*-test. (**E**) Average >200Hz amplitude correlation between co-ripples for each cortical channel-pair does not decrement with fiber tract distance.

Co-rippling increases putative unit-activity correlation between distant cortical sites

Our findings that co-ripples are often phase-locked across distant sites, and that unit-firing is phase-locked to local ripples, together imply that unit-firing is also correlated across distant sites. We were unable to test this prediction directly because we did not perform microelectrode recordings of units in multiple locations separated by more than ~5mm. Rather, as an indirect test, we used >200Hz amplitude from SEEG recordings as a proxy for unit-firing (31). During waking but not NREM, this measure was highly correlated when cortical sites were co-rippling vs. when they were not (Fig.5D, $p=8\times10^{-303}$, two-sided paired *t*-test). Correlation between co-rippling sites did not significantly decrement with increasing distance between the sites (Fig.5E; $r=-0.04$, $p=0.07$, significance of the correlation coefficient).

As described above, co-ripple phase-lags between channels tended to be near 0 or π, especially during waking. This could indicate that co-rippling sometimes represents a state of inhibited communication, or simply that our bipolar SEEG derivations had variable relationships to local ripple generating dipoles. To test these hypotheses, we compared the >200Hz amplitude correlations between sites, when the sites had co-ripple phase-lags of 0±π/6 vs. π±π/6 (averaged within these ranges for each channel-pair). No significant difference was found for waking or NREM (Waking: $p=0.17$; NREM: $p=0.07$, two-sided paired *t*-test, $N=2275$ channel pairs), thus suggesting that the lags near 0 and π are functionally equivalent as would be expected if they are due to slight differences in electrode location relative to cortical lamina.

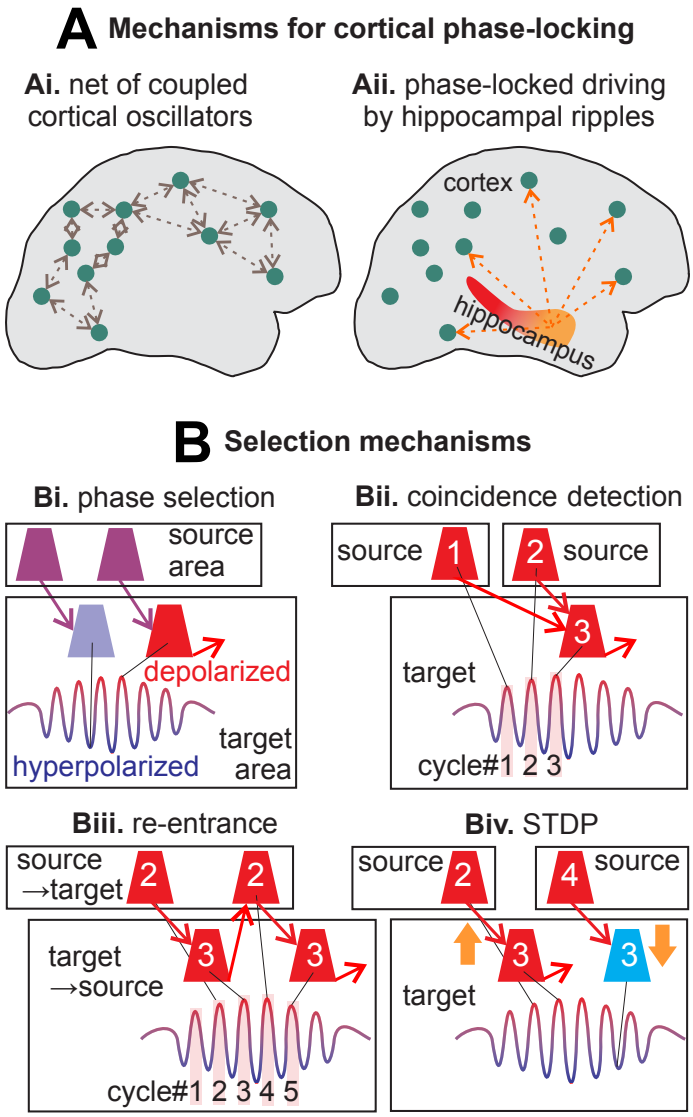

Fig. 6. Mechanisms of phase-locked networks of cortical ripples and their selection. (**A**) Potential mechanisms for ripple phase-locking across broad cortical regions: (**Ai**) multiple cortico-cortical re-entrant connections between the cortical oscillators; (**Aii**) distributed driving oscillations from a subcortical location (e.g., hippocampal ripples). (**B**) Multiple synergistic mechanisms enabled by cortico-cortical co-rippling could select a spatiotemporal neural network. (**Bi**) Spikes arriving at the hyperpolarized phase will be ineffective relative to those arriving at the depolarized phase in eliciting spikes in the rippling target area. (**Bii**) Coincident spikes arriving from two source areas that are phase-locked with the target area are more likely to trigger an action-potential, especially if they arrive in the depolarized phase. Note that conduction times between areas does not need to match the phase-lag but could equal the phase-lag plus multiples of the cycle time (e.g., cell #1→3). (**Biii**) Re-entrant activation across cycles could also result from reciprocal connections. (**Biv**) The synapses effectively evoking spikes (2→3) would be strengthened with spike-timing-dependent plasticity (STDP), whereas those arriving from a non-phase-locked area (4→3) would arrive after the target cell fires and thus be weakened. Whereas the mechanisms in (Bi-iii) would act synergistically to reinforce in-phase firing between co-rippling sites within a given ripple, the mechanism in (Biv) would act across ripples to reinforce a particular network of co-rippling sites.

Discussion

Here, using human intracortical recordings, we show that ripples couple, co-occur, and phase-synchronize across all lobes and between both hemispheres, with little decrement, even at long distances. The rate of co-rippling above chance increased exponentially with the proportion of co-rippling sites, which was correlated with stronger phase-locking. Cortical neurons increased firing during ripples and phase-locked to them, a requisite for ripples to enhance interaction via gain-modulation and coincidence detection. Enhanced long-distance interaction during co-rippling between sites was supported by increased high-frequency correlation. In addition to spontaneously occurring during both NREM and waking, cortico-cortical and hippocampo-cortical ripple co-occurrence specifically increased preceding successful delayed recall. Overall, our results suggest that distributed, phase-locked cortical ripples possess the properties that may allow them to facilitate integration of the different elements comprising a particular declarative memory, or more generally, to help 'bind' different aspects of a mental event encoded in widespread cortical areas into a coherent representation.

Previous work showed that coupling of anterolateral temporal and parahippocampal ripples in humans increases prior to correct recall in paired-associates learning (8). We show that such coupling also occurs between hippocampal and cortical ripples. Further, we show that immediate recall with no intervening distractor, a task with identical sensory and motor stimulation but that does not require the hippocampus (12), is not associated with increased hippocampo-cortical ripple coupling. Critically, given the importance of transcortical connections between sites encoding previously unrelated elements in declarative memory, we show that cortico-cortical ripple coupling also strongly increases prior to correct recall following a delay.

In addition to consolidation during sleep, the hippocampus is needed for memory formation during waking, as demonstrated by transient medial temporal inactivation (32). Indeed, we found that spontaneous hippocampal ripples were more tightly coupled with cortical ripples in waking compared to NREM. However, unlike NREM, during which 67% of hippocampo-cortical channel-pairs with a significant order preference had hippocampal ripples preceding cortical, during waking the opposite was true, with cortex leading in 85%. While speculative, these observations are consistent with the cortex generally providing information to the hippocampus for encoding during waking (when hippocampal ripples follow cortical), and then the hippocampus providing information to the cortex for consolidation during NREM (when hippocampal ripples precede cortical).

A novel finding of this study is that spontaneous cortical ripples couple (within ±500ms), co-occur (≥25ms overlap), and often phase-lock (synchronize) across large areas of both hemispheres during both sleep and waking. The minimal decrement with distance in co-occurrence or phase-locking suggests either a central driving oscillator, or a population origin, such as a web of coupled oscillators (Fig.6A). The hippocampus is unlikely to act as a central driving oscillator because hippocampo-cortical coupling and co-rippling is rarer than cortico-cortical, and hippocampo-cortical phase-locking is essentially absent. A preponderance of cortico-cortical influences might be expected given that each cortical pyramidal cell receives input from thousands of other pyramids, whereas the fan-out from hippocampus (CA1 plus subiculum) to cortex is ~1:500, so each cortical pyramid gets on average less than 10 hippocampal synapses (33, 34).

Conversely, a network of coupled oscillators is consistent with the finding in cats that section of the corpus callosum disrupts gamma-synchrony between V1 in the two hemispheres (17). Furthermore, the highly uniform ripple frequency observed across sites, cortical regions, and

individual ripples suggests that local cellular and network mechanisms set the resonant oscillation frequency of each cortical module to the same 80Hz frequency, which are thereby prone to co-oscillate when excited and connected. A major role of cortico-cortical interactions in ripple co-occurrence and phase-locking is also suggested by the strong positive feedback we observed in the spread of cortico-cortical co-occurrence and the intensity of cortico-cortical phase-locking. Specifically, cortico-cortical co-occurrence probability during waking increases from about twice chance levels for two co-occurring sites to about 20,000 times chance for co-occurrence in 25% of the sites. Similarly, during NREM, peak cortical ripple PLV between sites increases linearly with the number of additional sites co-rippling, from ~0.2 with no additional sites to ~0.9 with twelve. Note that a PLV of 1.0 would indicate perfect consistency of phase between sites over all of their co-occurring ripples.

It may seem unlikely that cortico-cortical interactions could support zero-lag phase-locking at long distances, with minimal decrement up to 250mm as was demonstrated here. Cortico-cortical fibers are unlikely to conduct much faster than 10m/s, or 125mm between successive peaks of an 80Hz ripple (35). However, synchronizing projections can still be effective at multiples of the cycle time, especially with recurrent connectivity (Fig.6B), as is typical in the cortex. Actually, since long-range fibers are quite rare in human cortex, whereas local connectivity and U-fibers are dense, an astronomical number of possible multi-synaptic routes exist between any two cortical locations. Indeed, modelling studies show that phase-locked oscillations at ~80Hz can occur in extended cortical networks, even at zero lag, provided that the neurons have multiple-path recurrent connectivity (36, 37). Thus, although direct evidence is lacking, the most likely possibility given our findings is that ripples co-occur and phase-lock due to emergent cortico-cortical interactions.

We found that cortico-cortical co-rippling and phase-locking show consistent differences between states. Although spontaneous cortical ripple occurrence density is higher in NREM, co-occurrence density is higher in waking. Accordingly, the likelihood of multiple sites co-rippling relative to chance grows more rapidly with number of sites during waking than NREM, the increase being about 25 times larger when 25% of sites are co-rippling. Overall, the proportion of ripple peaks that occur within 25ms of each other is about five times greater in waking than NREM. Furthermore, when co-ripples phase-lock they are more likely to be effectively synchronous in waking than NREM. These properties are consistent with a rapid highly synchronous recruitment of multiple cortical sites by a high activation during waking ripples, and by contrast, a sequential activation of NREM ripples. Higher activation is indicated by the greater increase in >200Hz amplitude during waking compared to NREM ripples. Conversely, NREM ripples tend to recruit sequentially across the cortex, with an increase in associated cell-firing.

A mean of about 16 widely-distributed cortical locations were sampled per patient. Assuming that a ripple generating module spans ~1mm^2 of cortical surface (unpublished data), this indicates that we recorded from only ~1/10000th of the ripple modules. If the distances between a significant number of recording sites were less than the size of rippling modules, then there would be increased co-rippling found at short inter-contact distances. The absence of such an effect allows the proportion of recorded sites to be used as an estimate of the proportion of the cortex that is rippling. If so, then at times, as much as 25% of the cortex is co-rippling. Similarly, the usual proportion of the cortex co-rippling can be roughly estimated from the probability, given a ripple, that another site is co-rippling, ~8% (assuming that the ripple's lead-field is comparable to its module size).

Given the strong ripple phase-modulation of cell-firing we demonstrated, ripples can be expected to strongly modulate the effectiveness of arriving synaptic input, with spikes arriving on the depolarized phase being far more likely to trigger post-synaptic firing. Thus, there may be a strong selection for cells that project (even multi-synaptically) between co-rippling sites with a latency matching the phase-lag (possibly plus multiples of the cycle time, Fig.6Bi). Additionally, when multiple sites co-ripple, then spikes that arrive together at a third location may have greatly enhanced effectiveness (i.e., the post-synaptic site acts as a coincidence detector, Fig.6Bii) (38). Synaptic phase-selection and coincidence detection are synergistic, and would further imply positive feedback due to recurrence (Fig.6iii). Connectivity between co-rippling locations supporting in-phase interactions would be progressive because the pre- and post-synaptic activation these mechanisms induce would strengthen in-phase connections via STDP (Fig.6Biv). Note the requisite pre-condition for this progressive strengthening of in-phase connections is that there is consistency of phase-lags across all waking or NREM co-ripples of a site-pair, which is what our criterion for phase-locking required. However, the gain-modulation and coincidence detection mechanisms would also function between sites that are co-rippling but not phase-locked according to our criterion, because cross-site phase is still consistent within each co-ripple due to the small range of ripple frequencies (50% within ~0.3Hz of the mean). Thus, through gain modulation and coincidence detection (18), co-rippling may strongly select the distributed cortical network active during a co-rippling event.

Through these mechanisms, cortical ripples could activate and couple with distant but related encoding areas through progressive activation of a web of cortico-cortical positive feedback connections. The strongly increased probability of co-activation and phase-locking with increasing numbers of contacts already co-activating suggests positive feedback recruitment of the most interconnected and co-activated cells into a brief synchronous ripple. When locations join the rippling network and resonate with other members, their activity level increases. The function of the ripple could thus be to act as an amplifier through resonance, leading to the rapid assembly of a network encoding the various aspects of an event.

A potential role of co-ripples in facilitating the communication and integration of information between distant cortical sites requires both the synchronized oscillations in trans-membrane currents generating the co-ripples *per se*, and coordinated neuronal action-potentials. We show here that single putative pyramidal and interneurons in lateral temporal cortex increase their firing during ripples in a manner that is strongly modulated by the phase of the individual ripple cycles. Therefore, the cell-firing patterns necessary to support selection of activated neurons within the co-rippling locations using gain modulation and coincidence detection are in place. While we did not simultaneously record single units in multiple distant locations to directly confirm that they are co-firing, we obtained some indication that this may be the case by examining the envelope of >200Hz local field potentials. We found that the correlation between these envelopes in distant locations is greater when they are co-rippling, and furthermore, this increase in correlation does not decrease with distance, even if the sites are in different lobes or hemispheres.

The principle alternative proposed mechanism for binding relies on hierarchical convergence in multi-attribute, multisensory areas (19, 20). This mechanism seems inconsistent with the highly distributed nature of cortical processing, and poses the difficulty how to pre-represent in a small cortical module each of the combinatorial possibilities of all elements contained in all potential experiences. However, the hippocampus seems to do this, albeit temporarily, with receptive fields that combine indicators of position from multiple modalities, as well as valence, history, and context (39). Hippocampal assembly of the different elements of an event does not require integration across the hippocampus because these elements are available locally, having been

pre-mixed by the entorhinal cortex and dentate gyrus. Thus, hippocampal ripples are for communication with the cortex rather than with other hippocampal sites, and indeed they are typically local within the hippocampus (22, 40); rather, their crucial co-occurrences may be with widespread cortical ripples. In this view, binding of cortical elements can occur in the absence of hippocampal input if they are previously consolidated, because cortico-cortical co-rippling and phase-locking are dependent on intracortical processes.

In summary, the characteristics of co-occurring and phase-locked cortical ripples found in the current study appear to fulfill the central requirements for a neurophysiological process that could faciliate binding-by-synchrony. First, ripples occur in all regions of the cortex in both hemispheres (required by binding because the elements of experience are encoded throughout the cortex). Second, ripples occur spontaneously throughout waking and NREM (required since binding is a ubiquitous process), and are elevated during task periods when binding may be useful (such as reassembling the components of a memory). Third, ripples last ~70ms, a duration considered in the range of 'the psychological moment' (41). Fourth, ripples strongly increase local firing and firing-proxy >200Hz amplitude (required for inter-areal communication). Fifth, ripples strongly phase-modulate local putative pyramidal and interneuron firing in a manner consistent with input modulation (a primary hypothesized mechanism whereby oscillations selectively amplify particular neural assemblies). Sixth, ripples strongly co-occur and phase-lock between cortical sites indicating active cortico-cortical communication (required because without communication there cannot be integration). This strong phase-locking occurs between cortical sites but not between cortex and hippocampus, indicating that trans-cortical synchrony is probably intrinsic, i.e., not projected from elsewhere. Furthermore, co-occurrence and phase-locking is minimally affected by distance (required for integration of diverse elements). Finally, >200Hz amplitude is more correlated between sites when they are co-rippling, further suggesting interareal integration of unit-firing. Additional evidence from simultaneous distributed cellular level recordings, as well as direct interventions in model systems, will be necessary to confirm that cortical co-ripples provide the neural substrate for binding.

Methods

Patient selection

Data from a total of 25 patients (13 female, 31±11 years old) with pharmaco-resistant epilepsy undergoing intracranial recording for seizure onset localization preceding surgical treatment were included in this study (STable 1,6). Patients whose stereoelectroencephalography (SEEG) recordings were analyzed were only included in the study if they had no prior brain surgery; background EEG (with the exception of epileptiform transients) in the normal range; and electrodes implanted in what was eventually found to be non-lesional, non-epileptogenic cortex, as well as non-lesional, non-epileptogenic hippocampus (such areas were suspected to be part of the focus prior to implantation, or were necessary to pass through to reach suspected epileptogenic areas).

In addition, 3 of these patients were also implanted with an intracranial microelectrode (Utah Array) into cortical tissue that was suspected based on pre-surgical evaluation to be included within the region of the therapeutic resection (STable 6). The implantation of the array did not affect clinical monitoring. In all patients, the tissue into which the array was implanted was later resected to gain access to the surgical focus beneath, the electrode was determined not to be

implanted in epileptogenic tissue, and seizures were determined not to originate from the area where the array was implanted.

Patients were excluded from the study if they had prior brain surgery or did not have non-lesioned hippocampal and cortical channels that were not involved in the early stage of the seizure discharge and did not have frequent interictal activity or abnormal local field potentials. Based on these criteria, 25 were included in this study out of a total of 83. All patients gave fully informed written consent for their data to be used for research as monitored by the local Institutional Review Boards at Cleveland Clinic, University of California, San Diego, Oregon Health & Science University, and Partners HealthCare (including Massachusetts General Hospital),

Intracranial recordings

Patients were implanted with intracranial electrodes for ~7 days with continuous recordings for seizure onset localization. SEEG electrode implantation and targeting were made for purely clinical purposes. SEEG recordings were collected with a Nihon Kohden JE-120 amplifier at 1000Hz sampling (patients S1-17), Natus Quantum LTM amplifier at 1024Hz (patients S18-19), or Natus Xltek EMU128FS (patients S20-22). Standard clinical electrodes were 0.8mm diameter, with 10-16 2mm long contacts at 3.5-5mm pitch (~150 contacts/patient). In addition, patients S19 and S22 had electrodes with 0.5-2mm long contacts at 1-2mm pitch.

Electrophysiology pre-processing

Offline data preprocessing was performed in MATLAB 2019b and LFPs were inspected visually using the FieldTrip toolbox (42). SEEG data were downsampled to 1000Hz with anti-aliasing and 60Hz notch filtered (zero-phase) with 60Hz harmonics up to 480 Hz. Transcortical contact pairs were identified using both anatomical location (using the pre-operative MRI aligned to the post-operative CT), and physiological properties (high amplitude, coherence and inversion of spontaneous activity between contacts), and selected such that no 2 pairs shared a contact, with the exception of the 1mm spaced hippocampal bipolar channels described above. All SEEG analyses were performed using bipolar derivations between contacts separated by 1-5 mm in cortical or hippocampal gray matter in order to ensure that activity was locally generated (43).

Channel selection

Channels were excluded from analysis if they were in lesioned tissue, involved in the early stages of the seizure discharge, had frequent interictal activity, or abnormal local field potentials. From the total 2772 bipolar channels (1326 left hemisphere) in the 22 SEEG patients (S1-22), 52 hippocampal (24 left hemisphere) and 403 transcortical (180 left hemisphere) bipolar channels were selected for the analyses (STable 1). Polarity was corrected for individual bipolar channels such that downstates were negative and upstates were positive. This was accomplished by ensuring that during NREM, negative peaks were associated with decreased, and positive peaks were associated with increased, mean ±100ms 70-190Hz analytic amplitude, an index of cell-firing that is strongly modulated by downstates and upstates (44).

Electrode localization

Cortical surfaces were reconstructed from the pre-operative whole-head T1-weighted structural MR volume using the standard FreeSurfer recon-all pipeline (45). Atlas-based automated

parcellation (46) was used to assign anatomical labels to regions of the cortical surface in the Destrieux (47) atlas. In addition, automated segmentation was used to assign anatomical labels to each voxel of the MR volume, including identifying voxels containing hippocampal subfields (48). In order to localize the SEEG contacts, the post-implant CT volume was registered to the MR volume, in standardized 1mm isotropic FreeSurfer space, using the general registration module (49) in 3D Slicer (50). The position of each SEEG contact, in FreeSurfer coordinates, was then determined by manually annotating the centroids of electrode contact visualized in the co-registered CT volume. Each transcortical contact pair was assigned an anatomical parcel from the atlas above by ascertaining the parcel identities of the surface vertex closest to the contact-pair midpoint. Subcortical contacts were assigned an anatomical label corresponding to the plurality of voxel segmentation labels within a 2-voxel radius. Transcortical contact pair locations were registered to the fsaverage template brain for visualization by spherical morphing (51). White-matter streamline distances between channels were computed using the 360 parcels of the HCP-MMP1.0 atlas (23), as determined by probabilistic diffusion MRI tractography (24), are population averages from (25). When two channels were in the same HCP parcel the distance was considered to be 0.

Time-frequency analyses

Average time-frequency plots of the ripple event-related spectral power (ERSP) were generated from the broadband LFP using EEGLAB (52). Event-related spectral power was calculated from 1Hz to 500Hz with 1Hz resolution with ripple centers at t=0 by computing and averaging fast Fourier transforms with Hanning window tapering. Each 1Hz bin of the time-frequency matrix was normalized with respect to the mean power at -2000 to -1500ms and masked with two-tailed bootstrapped significance (N=200) with FDR correction and α=0.05 using -2000 to -1500ms as baseline.

Sleep and waking epoch selection

Epochs included in the study did not fall within at least 1 hour of a seizure and were not contaminated with frequent interictal spikes or artifacts. NREM periods were selected from continuous overnight recordings where the delta (0.5-2Hz) analytic amplitude from the cortical channels was persistently increased (STable 1). Sleep epochs were confirmed by visual inspection to have normal appearing spindles, downstates, and upstates. Waking periods were selected from continuous daytime recordings that had persistently low cortical delta as well as high cortical alpha (8-12 Hz), beta (20-40Hz), and high gamma (70-190Hz) analytic amplitudes. When the data included electrooculography (EOG; N=15/17 SEEG patients S1-17), waking periods also required that the 0.5-40Hz analytic amplitude of the EOG trace was increased. Waking epochs were required to be separated from periods of increased delta analytic amplitude by at least 30 minutes.

Ripple detection

Ripple detection was performed in the same way for all structures and states and was based on a previously described hippocampal ripple detection method (21, 22). Requirements for inclusion and criteria for rejection were determined using an iterative process across patients, structures, and states. Data were bandpassed at 60-120Hz and the top 20% of 20ms moving root-mean-squared peaks were detected. It was further required that the maximum z-score of the analytic amplitude of the 70-100Hz bandpass was greater than 3 and that there were at least 3 distinct oscillation cycles in the 120Hz lowpassed signal, determined by shifting a 40ms window in increments of 5ms across ±50ms relative to the ripple midpoint and requiring that at

least 1 window have at least 3 peaks. Adjacent ripples within 25ms were merged. Ripple centers were determined as the time of the maximum positive peak in the 70-100Hz bandpass. To reject epileptiform activities or artifacts, ripples were excluded if the absolute value of the z-score of the 100Hz highpass exceeded 7 or if they occurred within 2s of a ≥1mV/ms change in the LFP. Ripples were also excluded if they fell within ±500ms of putative interictal spikes, detected as described below. To exclude events that could be coupled across channels due to epileptiform activity, we excluded ripples that coincided with a putative interictal spike on any cortical or hippocampal channel included in the analyses. Events that had only one prominent cycle or deflection in the broadband LFP that manifested as multiple cycles above detection threshold in the 70-100Hz bandpass were excluded if the largest valley-to-peak or peak-to-valley absolute amplitude in the broadband LFP was 2.5 times greater than the third largest. For each channel, the mean ripple-locked LFP and mean ripple band were visually examined to confirm that there were multiple prominent cycles at ripple frequency (70-100Hz) and the mean time-frequency plot was examined to confirm there was a distinct increase in power within the 70-100Hz band. In addition, multiple individual ripples in the broadband LFP and 70-100Hz bandpass from each channel were visually examined to confirm that there were multiple cycles at ripple frequency without contamination by artifacts or epileptiform activity. Channels that did not contain ripples that meet these criteria were excluded from the study.

Additional analyses were performed specifically on sharpwave-ripples and spindle-ripples detected according to our previous methods (21, 22). First, NREM data were bandpassed from 70-100Hz, and a putative ripple was detected when the 20ms moving root-mean-squared amplitude exceeded the 90th percentile. Ripples were required to have at least 3 distinct oscillation cycles as described above. Broadband LFP data ±2s around ripple centers underwent 1-D wavelet (Haar and Daubechies) decomposition to detect and remove sharp transients. Ripples were classified as sharpwave-ripples based on the similarity of the peri-ripple LFP to the 400ms average biphasic waveform template created for each subject using 100-300 hand-marked hippocampal sharpwave-ripples, as quantified by the dot product between the template and the peri-ripple LFP (-100 to 300ms), and the absolute difference between the LFP value at the ripple center. Ripples were classified as spindle-ripples if the ripple center occurred during a hippocampal spindle, detected in the same way as described below for cortical spindles, on the same channel. Ripples could be classified as both sharpwave-ripples and spindle-ripples if they met both of these criteria.

Interictal spike detection and rejection

Ripples and sleep graphoelements were excluded if they were within ±500ms from putative IIS detected as follows. A high frequency score was computed by smoothing the 70-190Hz analytic amplitude with a 20ms boxcar function and a spike template score was generated by computing the cross-covariance with a template interictal spike. The high frequency score was weighted by 13 and the spike score was weighted by 25, and an IIS was detected when these weighted sums exceeded 130. In each patient, detected IIS and intervening epochs were visually examined from hippocampal and cortical channels (when present) to confirm high detection sensitivity and specificity.

Paired-associates memory task

Paired-associates memory task data were collected from 5 patients using Presentation (Neurobehavioral Systems). Patients were instructed to memorize a series of word pairs and to recall the second word when cued with the first. A word pair was presented with text and audio (pre-recorded speech) along with an integrating image that contained semantic content of both

words. After each presentation, immediate recall was assessed by cuing the first word immediately after the offset of the word pair and image. The patient then attempted to recall the word aloud. This was repeated with 8 different pairs followed by a 6s break, and then delayed recall of the 8 pairs was assessed in the same order where the first word was cued and the patient attempted to recall the second word aloud. After 4s the integrating image was displayed. Delayed recall was only considered successful if the second word was said aloud before the image appeared. This sequence was repeated 20 times for a total of 160 word pairs. For one patient (S18), the task was instead structured as 25 sets of 6 pairs with the integrating image shown during the encoding period but not during delayed recall, and instead during delayed recall the second word was presented after 5s. Delayed recall was only considered successful for this patient if the second word was said aloud before it was presented after 5s. Task performance by patient is summarized in STable 4.

During the task, audio containing the stimulus presentations and patient voice was split and simultaneously recorded into the task presentation computer and into the clinical amplifier system synchronously with the intracranial recordings. Stimulus markers sent by the task computer were also synchronized with the intracranial recordings. Scoring of behavioral data was done offline by listening, and recall onsets were identified offline using Audacity v2.4.2 through both visual examination of the task computer recorded audio waveforms and spectrograms and confirmation through listening. The computer recorded audio was downsampled with anti-aliasing to 1000Hz and cross-correlated with the audio recorded alongside the intracranial recordings to ensure high temporal precision of recall onsets.

Ripple occurrences and co-occurrences relative to the word cue (text and audio) preceding recall onsets prior to successful (i.e., correct response before the answer or integrating image was presented in the delayed condition) or unsuccessful (i.e., no response, incorrect response, or response after the answer or image was presented) were computed across trials, where each trial was an average across channels. Null distributions of occurrences were computed by randomly shuffling ripple or co-occurring ripple centers for each channel in each trial within ±3s from cue onset 10 times. Observed over chance (average of null) ripple occurrence and co-occurrence histograms had 25ms bins Gaussian-smoothed with a 100ms window. Trial-wise ripple occurrence and co-occurrence averages in the 150-300ms window following cue onset were computed for statistical analyses.

Ripple temporal relationships

Peri-cortical ripple time histograms of cortical or hippocampal ripples on a different channel were computed. Gaussian smoothed (window=250ms) ripple center counts in channel B were computed in 25ms bins within ±1500ms relative to ripple centers at t=0 in channel A. A null distribution was generated by shuffling (N=200 times) the times of ripple centers on channel B relative to the ripple centers on channel A (at t=0) within the ±1500 window. Pre-FDR p-values were calculated by comparing the observed and null distributions for each bin over ±500ms. P-values were then FDR-corrected for the number of channel pairs across patients multiplied by the number of bins per channel pair (53). A channel pair was determined to have a significant modulation if there were at least 3 consecutive bins with FDR-corrected $p<0.05$. Whether cortical ripples were leading or lagging was determined using a two-sided binomial test with expected value of 0.5, using event counts in the 500ms before vs. 500ms after t=0. For plots, 50ms Gaussian smoothed event counts with 50ms bins were used.

Cortical ripple co-occurrences

Ripple co-occurrences between channel pairs were identified by finding ripples that overlapped for at least 25ms. The center of the co-occurring ripple event was determined by finding the temporal center of the ripple overlap. Conditional probabilities of ripple co-occurrence were computed by finding the probability of co-occurrence (minimum 25ms overlap) between two channels given that there was a ripple in one of the channels, separately for each channel. This was done for P(NC|NC) (both orders), P(NC|HC), and P(HC|NC). To estimate the extent of co-rippling across the cortex at any moment, the probability that a given proportion of channels was co-rippling at any time point for each subject was computed.

Observed over chance cortical ripple co-occurrence was computed as a function of the number of sites co-rippling. Ripple co-occurrence of a given number of sites required that all of those sites had at least 25ms ripple overlap. Chance was computed for each patient by randomly shuffling the ripple epochs and inter-ripple epochs of all sites 200 times and calculating the mean number of co-occurrences for each proportion of co-rippling sites (i.e., the number of channels co-rippling divided by the total number of channels, assessed for the minimum value of 2 or more channels co-rippling).

Cortical ripple co-occurrence significance for each channel pair was computed by comparing the number of observed co-occurrences (25ms minimum overlap) for each channel pair with a null co-occurrence distribution derived from shuffling ripples and inter-ripple intervals 200 times in a moving non-overlapping 5min window and counting co-occurrences.

Ripple phase-locking analyses

To evaluate the extent to which co-occurring ripples at different sites were synchronized at different times, we used the phase-locking value (PLV), an instantaneous measure of phase-locking (28). PLV time courses were computed using the analytic angle of the Hilbert transformed 70-100Hz bandpassed (zero-phase shift) signals of each channel pair when there were at least 40 co-ripples with a minimum of 25ms overlap for each. PLVs were computed for all such co-ripples for each channel pair across a ±500ms window relative to the temporal centers of the co-ripples. A null distribution was generated by selecting 200 random times within -10 to -2 s relative to each co-ripple center. For plotting, PLV traces were smoothed with a 10ms Gaussian window. Pre-FDR p-values were determined by comparing the observed and null distributions in 5ms duration bins within ±50ms around the co-ripple centers. These p-values were then FDR corrected across bins and channel pairs. A channel pair was considered to have significant phase-locking if it had 2 consecutive bins with post-FDR $p<0.05$. Phase-locking modulation was computed for each channel pair as the difference from the average baseline PLV within -500 to -250ms to the max PLV within ±50ms around the co-ripple center. Phase-locking as a function of the proportion of additional sites co-rippling was computed by identifying co-ripples on the two cortical channels of interest, then sorting these events into groups based on what proportion of additional sites had a ripple that overlapped with the co-ripple by any amount of time, and computing the peak PLV and ΔPLV around the co-ripple centers. Plots of the peak PLV for channel pairs as a function of the number of additional sites co-occurring (e.g., 3 on the x-axis means 2+3=5 total sites co-rippling) are for channel pairs with significant PLV modulations.

Ripple phase-lag analyses

The phase-lag between co-occurring cortical ripples (25ms minimum overlap) was computed for channels with significant PLV modulations (see above) by finding the circular mean (54) of the angular difference between the two 70-100Hz bandpassed ripples during their overlapping period. The mean phase-lag for a given channel pair was computed by finding the circular mean of these circular means. For each channel pair that had a significant PLV modulation, differences in ripple phase-lags by sleep night were computed for each sleep night pair where both nights had at least 30 co-ripples using the Watson-Williams multi-sample test for equal means.

Unit detection, classification, quality, and isolation

Unit detection and classification was performed according to our published procedures (55-61). Data were bandpassed at 300-3000Hz and putative unit spikes were detected when the filtered signal exceeded 5 times the estimated standard deviation of the background noise. Units were k-means clustered using the first three principal components of each spike. Overlaid spikes were examined visually and those with abnormal waveforms were excluded. Based on their waveforms, firing rates, and autocorrelograms, action potentials were clustered as arising from putative pyramidal cells or interneurons. Putative pyramidal cells had spike rates of ~0.1-0.8Hz, long valley-to-peak and half width intervals, sharp autocorrelations, and bimodal inter-spike interval (ISI) distributions, reflecting a propensity to fire in bursts (STable 6). By contrast, putative interneurons had spike rates of ~1-5Hz, short valley-to-peak and half width intervals, broad autocorrelations, and a predominantly unimodal ISI distribution.

Single unit quality and isolation were confirmed according to previously established guidelines (62). Unit spikes were verified to well-exceed the noise floor based on large peak signal-to-noise ratios (PY: 9.12±3.39; IN: 5.23±2.88). Since the neuronal spiking refractory period is about 3ms, the percent of ISIs less than 3ms estimates the degree of single unit contamination by spikes from different units, which was very low among the units included in this study (PY: 0.21±0.34%; IN: 0.33±0.58%). Furthermore, single units detected on the same contact were highly separable according to their projection distances (30) (PY: 95.38±86.00 SD; IN: 82.84±83.35 SD). Lastly, temporal stability of unit spikes over time was confirmed based on consistency of the mean waveform shape and amplitude of each unit across recording quartiles.

Analyses of unit spiking during ripples

Unit spiking was analyzed with respect to local ripples detected on the same contact. Ripple phases of unit spikes were determined by finding the angle of the Hilbert transform of the 70-100Hz bandpassed signal (zero-phase shift) at the times of the spikes. Unit spiking modulations during ripples were computed by comparing the number of spikes for each unit during ripples divided by the number during non-ripple epochs, i.e., epochs in between ripples, that were matched in number and duration to the ripples.

Statistical analyses

All statistical tests were evaluated with $\alpha=0.05$. All p-values involving multiple comparisons were FDR-corrected according to Benjamini and Hochberg (1995)(53). FDR corrections across channel pairs were done across all channels pairs from all patients included in the analysis. Box-and-whisker plots show median, mean, and interquartile range, with whiskers indicating 1.5

× interquartile range with outliers omitted. Significance of linear correlations were assessed using the significance of the correlation coefficient when there were at least 10 data points.

In temporal analyses (i.e., peri-ripple time histograms), p-values were corrected across bins and all channels. To compute p-values using randomization tests, the observed test statistic (e.g., events per bin) was compared to the null distribution of test statistics. Null distributions were randomly selected from the same epochs using 200 iterations. The p-value was computed as the proportion of null test statistics that were equal to or greater/less than the observed test statistic. Randomization tests were one-sided according to whether the observed test statistic was greater than or less than the mean of the null test statistics. Order preferences (e.g., of ripples between channels) were assessed using a two-sided binomial test with an expected probability of 0.5. To determine if a circular distribution was non-uniform, the Hodges-Ajne test was used. To determine if two circular distributions had different circular means, a Watson-Williams multi-sample test was used. To test if co-rippling between two particular cortical sites made it more likely that additional cortical sites co-rippled, we computed a χ^2 test of proportions for all possible groups of three cortical channels under the null hypothesis that the co-occurrence of channel A and B has no relation to the co-occurrence of A and C. Each table was made from the number of ripples in A that co-occurred with a ripple in B only, or C only, or both, or neither, where A occurring with B or not B are the 2 rows, and A occurring with C or not C are the 2 columns.

In the paired-associates memory analysis, chance ripple occurrences (or co-occurrences) were computed for each trial as the average of 200 random shuffles per channel (pair) within ±3s from recall onset. Only trials where there was a successful recall (of the same word pair) in both the immediate and ~60s delayed conditions were included. Linear mixed-effects models were performed with the patient as the random effect, as follows:

$$\textit{(co-)ripples} \sim \textit{condition} + (1 \mid \textit{patient}) \qquad (1)$$

Where *(co-)ripples* was the dependent variable computed as the average ripple rate (or co-ripple rate; minimum of 25ms overlap for each co-ripple) within 150-300ms following the stimulus cue preceding successful recall onset across trials, with the value for each trial as the average across channels, *condition* was 1) immediate recall or chance, 2) delayed recall or chance, 3) immediate recall or delayed recall (as a ratio of observed over chance), or 4) successful recall or unsuccessful recall (as a ratio of observed over chance).

Linear mixed-effects models with the same structure as the one described above, with the patient as a random effect, were used to evaluate channel pair co-ripple metrics (co-occurrence probabilities, PLV modulations, and proportion of pairs with significant PLV modulations) with respect to fiber tract distance.

Differences in co-ripple phase-lag preferences between nights was assessed using the Watson-Williams multi-sample test for equal means. To test if unit spiking increase during ripples, a two-sample two-sided *t*-test was used to compare the spike counts during ripples vs. the spike counts during baseline periods selected in between ripples, which were matched in number and duration to the ripples. Ripple phase-modulations of spiking for each unit with at least 30 spikes during local ripples was assessed by comparing counts within $0 \pm \pi/2$ vs. $\pi \pm \pi/2$, with an expected value of 0.5.

Data availability

The de-identified raw data that support the findings of this study are available from the corresponding authors upon reasonable request provided that the data sharing agreement and patient consent permit that sharing.

Code availability

The code that support the findings of this study are available from the corresponding authors upon reasonable request.

References

1. M. A. Wilson, B. L. McNaughton, Reactivation of hippocampal ensemble memories during sleep. *Science* **265**, 676-679 (1994).
2. G. Buzsaki, Hippocampal sharp wave-ripple: A cognitive biomarker for episodic memory and planning. *Hippocampus* **25**, 1073-1188 (2015).
3. N. Maingret, G. Girardeau, R. Todorova, M. Goutierre, M. Zugaro, Hippocampo-cortical coupling mediates memory consolidation during sleep. *Nature Neuroscience* **19**, 959-964 (2016).
4. V. Ego-Stengel, M. A. Wilson, Disruption of ripple-associated hippocampal activity during rest impairs spatial learning in the rat. *Hippocampus* **20**, 1-10 (2009).
5. D. Khodagholy, J. N. Gelinas, G. Buzsáki, Learning-enhanced coupling between ripple oscillations in association cortices and hippocampus. *Science* **358**, 369-372 (2017).
6. F. Grenier, I. Timofeev, M. Steriade, Focal synchronization of ripples (80-200 Hz) in neocortex and their neuronal correlates. *J Neurophysiol* **86**, 1884-1898. (2001).
7. Y. Norman *et al.*, Hippocampal sharp-wave ripples linked to visual episodic recollection in humans. *Science* **365**, eaax1030 (2019).
8. A. P. Vaz, S. K. Inati, N. Brunel, K. A. Zaghloul, Coupled ripple oscillations between the medial temporal lobe and neocortex retrieve human memory. *Science* **363**, 975-978 (2019).
9. A. P. Vaz, J. H. Wittig, S. K. Inati, K. A. Zaghloul, Replay of cortical spiking sequences during human memory retrieval. *Science* **367**, 1131-1134 (2020).
10. N. Nitzan *et al.*, Propagation of hippocampal ripples to the neocortex by way of a subiculum-retrosplenial pathway. *Nature Communications* **11**, 1947 (2020).
11. C. W. Dickey *et al.*, Cortical ripples provide the conditions for consolidation during NREM sleep in humans. *bioRxiv (in process)* (2021).
12. L. R. Squire, Memory and the hippocampus: A synthesis from findings with rats, monkeys and humans. *Psychological Review* **99**, 195-231 (1992).
13. A. Treisman, Solutions to the binding problem: progress through controversy and convergence. *Neuron* **24**, 105-110, 111-125 (1999).
14. A. Revonsuo, J. Newman, Binding and Consciousness. *Consciousness and Cognition* **8**, 123-127 (1999).
15. C. von der Malsburg, The what and why of binding: the modeler's perspective. *Neuron* **24**, 95-104, 111-125 (1999).
16. C. M. Gray, P. Konig, A. K. Engel, W. Singer, Oscillatory responses in cat visual cortex exhibit inter-columnar synchronization which reflects global stimulus properties. *Nature* **338**, 334-337 (1989).
17. P. Uhlhaas *et al.*, Neural synchrony in cortical networks: history, concept and current status. *Frontiers in Integrative Neuroscience* **3** (2009).

18. P. Fries, Neuronal Gamma-Band Synchronization as a Fundamental Process in Cortical Computation. *Annual Review of Neuroscience* **32**, 209-224 (2009).
19. M. N. Shadlen, J. A. Movshon, Synchrony unbound: a critical evaluation of the temporal binding hypothesis. *Neuron* **24**, 67-77, 111-125 (1999).
20. B. Merker, The efference cascade, consciousness, and its self: naturalizing the first person pivot of action control. *Front Psychol* **4**, 501 (2013).
21. X. Jiang, J. Gonzalez-Martinez, E. Halgren, Coordination of Human Hippocampal Sharpwave Ripples during NREM Sleep with Cortical Theta Bursts, Spindles, Downstates, and Upstates. *J Neurosci* **39**, 8744-8761 (2019).
22. X. Jiang, J. Gonzalez-Martinez, E. Halgren, Posterior hippocampal spindle-ripples co-occur with neocortical theta-bursts and down-upstates, and phase-lock with parietal spindles during NREM sleep in humans. *J Neurosci* 10.1523/jneurosci.2858-18.2019, 2858-2818 (2019).
23. M. F. Glasser *et al.*, A multi-modal parcellation of human cerebral cortex. *Nature* (2016).
24. T. E. J. Behrens, H. J. Berg, S. Jbabdi, M. F. S. Rushworth, M. W. Woolrich, Probabilistic diffusion tractography with multiple fibre orientations: What can we gain? *NeuroImage* **34**, 144-155 (2007).
25. B. Q. Rosen, E. Halgren, A whole-cortex probabilistic diffusion tractography connectome. *eNeuro* 10.1523/eneuro.0416-20.2020, ENEURO.0416-0420.2020 (2021).
26. D. J. Felleman, D. C. VanEssen, Distributed hierarchical processing in the primate cerebral cortex. *Cerebral Cortex* **1**, 1-47 (1991).
27. M. F. Glasser, D. C. Van Essen, Mapping human cortical areas in vivo based on myelin content as revealed by T1- and T2-weighted MRI. *J Neurosci* **31**, 11597-11616 (2011).
28. J. P. Lachaux, E. Rodriguez, J. Martinerie, F. J. Varela, Measuring phase synchrony in brain signals. *Hum Brain Mapp* **8**, 194-208 (1999).
29. E. M. Izhikevich, Y. Kuramoto, "Weakly Coupled Oscillators" in Encyclopedia of Mathematical Physics*,* J.-P. Françoise, G. L. Naber, T. S. Tsun, Eds. (Academic Press, Oxford, 2006), 10.1016/B0-12-512666-2/00106-1, pp. 448-453.
30. C. Pouzat, O. Mazor, G. Laurent, Using noise signature to optimize spike-sorting and to assess neuronal classification quality. *Journal of Neuroscience Methods* **122**, 43-57 (2002).
31. R. Mukamel *et al.*, Coupling between neuronal firing, field potentials, and FMRI in human auditory cortex. *Science* **309**, 951-954 (2005).
32. E. Halgren, "Insights from evoked potentials into the neuropsychological mechanisms of reading" in Neurobiology of Cognition*,* A. Scheibel, A. Weschsler, Eds. (Guilford, New York, 1990), pp. 103-150.
33. G. Simić, I. Kostović, B. Winblad, N. Bogdanović, Volume and number of neurons of the human hippocampal formation in normal aging and Alzheimer's disease. *J Comp Neurol* **379**, 482-494 (1997).
34. F. A. Azevedo *et al.*, Equal numbers of neuronal and nonneuronal cells make the human brain an isometrically scaled-up primate brain. *J Comp Neurol* **513**, 532-541 (2009).
35. S. G. Waxman, H. A. Swadlow, The conduction properties of axons in central white matter. *Prog Neurobiol* **8**, 297-324 (1977).
36. M. Bazhenov, N. F. Rulkov, I. Timofeev, Effect of synaptic connectivity on long-range synchronization of fast cortical oscillations. *J Neurophysiol* (2008).
37. R. Vicente, L. L. Gollo, C. R. Mirasso, I. Fischer, G. Pipa, Dynamical relaying can yield zero time lag neuronal synchrony despite long conduction delays. *Proceedings of the National Academy of Sciences* **105**, 17157-17162 (2008).
38. E. Salinas, T. J. Sejnowski, Correlated neuronal activity and the flow of neural information. *Nat Rev Neurosci* **2**, 539-550 (2001).

39. H. Eichenbaum, Time cells in the hippocampus: a new dimension for mapping memories. *Nature Reviews Neuroscience* **15**, 732-744 (2014).
40. J. Patel, E. W. Schomburg, A. Berényi, S. Fujisawa, G. Buzsáki, Local Generation and Propagation of Ripples along the Septotemporal Axis of the Hippocampus. *J Neurosci* **33**, 17029-17041 (2013).
41. M. Wittmann, *Wenn die Zeit stehen bleibt. Kleine Psychologie der Grenzerfahrungen* (Verlag C.H.Beck, ed. 1, 2015).
42. R. Oostenveld, P. Fries, E. Maris, J. M. Schoffelen, FieldTrip: Open source software for advanced analysis of MEG, EEG, and invasive electrophysiological data. *Comput Intell Neurosci* **2011**, 156869 (2011).
43. R. A. Mak-McCully *et al.*, Distribution, Amplitude, Incidence, Co-Occurrence, and Propagation of Human K-Complexes in Focal Transcortical Recordings(1,2,3). *eNeuro* **2** (2015).
44. R. Csercsa *et al.*, Laminar analysis of slow wave activity in humans. *Brain* **133**, 2814-2829 (2010).
45. B. Fischl, FreeSurfer. *Neuroimage* **62**, 774-781 (2012).
46. B. Fischl *et al.*, Automatically parcellating the human cerebral cortex. *Cereb Cortex* **14**, 11-22 (2004).
47. C. Destrieux, B. Fischl, A. Dale, E. Halgren, Automatic parcellation of human cortical gyri and sulci using standard anatomical nomenclature. *NeuroImage* **53**, 1-15 (2010).
48. J. E. Iglesias *et al.*, A computational atlas of the hippocampal formation using ex vivo, ultra-high resolution MRI: Application to adaptive segmentation of in vivo MRI. *Neuroimage* **115**, 117-137 (2015).
49. H. Johnson, G. Harris, K. Williams, BRAINSFit: mutual information rigid registrations of whole-brain 3D images, using the insight toolkit. *Insight J* (2007).
50. A. Fedorov *et al.*, 3D Slicer as an image computing platform for the Quantitative Imaging Network. *Magn Reson Imaging* **30**, 1323-1341 (2012).
51. B. Fischl, M. I. Sereno, R. B. Tootell, A. M. Dale, High-resolution intersubject averaging and a coordinate system for the cortical surface. *Hum Brain Mapp* **8**, 272-284 (1999).
52. A. Delorme, S. Makeig, EEGLAB: an open source toolbox for analysis of single-trial EEG dynamics including independent component analysis. *Journal of Neuroscience Methods* **134**, 9-21 (2004).
53. Y. Benjamini, Y. Hochberg, Controlling the False Discovery Rate: A Practical and Powerful Approach to Multiple Testing. *Journal of the Royal Statistical Society. Series B (Methodological)* **57**, 289-300 (1995).
54. P. Berens, CircStat: a MATLAB toolbox for circular statistics. *J Stat Softw* **31**, 1-21 (2009).
55. C. W. Dickey *et al.*, Travelling spindles create necessary conditions for spike-timing-dependent plasticity in humans. *Nature Communications* **12**, 1027 (2021).
56. J.-B. Eichenlaub *et al.*, Replay of Learned Neural Firing Sequences during Rest in Human Motor Cortex. *Cell Reports* **31**, 107581 (2020).
57. B. Teleńczuk *et al.*, Local field potentials primarily reflect inhibitory neuron activity in human and monkey cortex. *Scientific reports* **7**, 40211 (2017).
58. M. Le Van Quyen *et al.*, High-frequency oscillations in human and monkey neocortex during the wake–sleep cycle. *Proceedings of the National Academy of Sciences* **113**, 9363-9368 (2016).
59. N. Dehghani *et al.*, Dynamic balance of excitation and inhibition in human and monkey neocortex. *Scientific Reports* **6** (2016).
60. A. M. Chan *et al.*, Speech-specific tuning of neurons in human superior temporal gyrus. *Cereb Cortex* **24**, 2679-2693 (2014).

61. A. Peyrache *et al.*, Spatiotemporal dynamics of neocortical excitation and inhibition during human sleep. *Proceedings of the National Academy of Science* **109**, 1731-1736 (2012).
62. J. Kamiński, A. Brzezicka, A. N. Mamelak, U. Rutishauser, Combined Phase-Rate Coding by Persistently Active Neurons as a Mechanism for Maintaining Multiple Items in Working Memory in Humans. *Neuron* **106**, 256-264.e253 (2020).